JOURNAL OF SPACECRAFT AND ROCKETS
Vol. 35, No. 5, September–October 1998

Detailed Computation of Ultraviolet Spectra in Rarefied Hypersonic Flow

Koffi K. Kossi* and Iain D. Boyd†
Cornell University, Ithaca, New York 14853

A new nonequilibrium radiation model is described that predicts the ultraviolet spectrum of hydroxyl (OH) from the electronic transition $A \rightarrow X$ for flow conditions corresponding to the bow-shock ultraviolet 2 flight experiment. Unlike previous studies, the new model includes the direct analysis of the electronically and vibrationally excited states, OH(A, $v' = 0, 1, 2$), of OH in the flowfield simulations. The flowfield is analyzed using the direct simulation Monte Carlo method. Results are presented for the altitude range of 80–100 km, where the Knudsen number varies from 0.036 to 1.3. The computation uses algorithms that improve the numerical resolution of the excited states that typically occur at mole fractions of 10^{-15}. The collisional transfer of rotational and vibrational energies of the electronic state, OH(A), are also studied in detail. It is demonstrated that the usual assumption made in continuum radiation models, that the rotational and vibrational temperatures of the electronically excited state are the same as those of the ground state of the bulk flow, fails. An important improvement is achieved in the spectral prediction using the new nonequilibrium radiation model, and good agreement is obtained between flight data and emission predictions over a range of altitudes.

Nomenclature

A = excited electronic state designation or reaction rate constant, m^3 molecule^{-1} s^{-1}
c = speed of light, m s^{-1}
E = activation energy or energy level of state, J
F' = rotational energy, m^{-1}
G' = vibrational energy, m^{-1}
g = statistical weight
H = altitude, km
h = Planck's constant, 6.625×10^{-34}, J s
J' = rotational quantum number
K = rate coefficient, m^3 molecule^{-1} s^{-1}
k = Boltzmann constant, 1.38×10^{-23}, J K^{-1}
M = a third body species
N = species number of particles or temperature exponent in rate coefficient expression
n = species number density, m^{-3}
Q = partition function
T_r = rotational temperature, K
T_t = translational temperature, K
T_v = vibrational temperature, K
t = time, s
V = cell volume, m^3
W = particle weight
X = ground electronic state designation or mole fraction
θ = vibrational characteristic temperature, K
ν = frequency, Hz
ρ = mass density, kg m^{-3}
τ = lifetime or vibrational relaxation time, s

Subscripts

e = electronic index
i = particle index
r = rotation index
s = species index
t = translation index
u = electronic upper state index
v = vibration index
v' = upper vibrational state
x = colliding particle
0, 1, 2 = excited states index
∞ = initial condition

Superscripts

diss = dissociation
ex = exchange
form = formation
qu = quenching
[ ] = concentration annotation

Received Jan. 12, 1998; revision received April 14, 1998; accepted for publication April 17, 1998.

*Research Associate, Department of Mechanical and Aerospace Engineering.
†Associate Professor, Department of Mechanical and Aerospace Engineering. Member AIAA.

Introduction

ULTRAVIOLET diagnostic experiments have been carried out to measure the intensity and spectral distribution of the radiation emitted from the shock wave of a missile flying at 5.1 km/s, the bow-shock ultraviolet 2 flight experiment (BSUV-2),[1] and to validate aerodynamics and radiation transfer models related to re-entry conditions. Detailed spectral measurements from BSUV-2 are available from about 110 to 71 km with uncertainty of a factor of about 2 (Ref. 1). The Knudsen number range for flow over the 10-cm radius nose of BSUV-2 varies from about 1 to 0.001. Therefore, numerical simulation of these flows is difficult due to the thermochemical nonequilibrium conditions, and the emission prediction signatures can be in error by orders of magnitude. In a previous paper,[2] we discussed the prediction of ultraviolet emissions radiated by hydroxyl (OH) for hypersonic nonequilibrium flow conditions corresponding to BSUV-2 (Ref. 1). The study obtained flowfield solutions that include the direct analysis of the electronically excited state species of OH using the direct simulation Monte Carlo (DSMC) method. Then the emission was predicted from the flowfield solutions using the nonequilibrium radiation code NEQAIR.[3,4] The present investigation continues these studies with the development of a reliable method for predicting the signatures, with the goal of breaking new ground by including the production and quenching of the electronically and vibrationally excited states, OH(A, $v' = 0, 1, 2$), directly in the DSMC flowfield simulations. The effect of rarefaction and the extremely small mole fractions of the radiating species, about 10^{-9}, have required the development of new algorithms that improve the numerical resolution of the trace species.[2] A further goal of the present study is to take advantage of the direct analysis of the electronic state species to study in detail its rotational and vibrational energies. This allows assessment of the usual assumption

made in NEQAIR that the rotational and vibrational temperatures of the excited state species are the same as those of the bulk flow or of the ground state species.

To perform the spectral computation, one must first know the number density of the electronically, vibrationally, and rotationally excited states. In the case of an equilibrium condition, this number density is determined from the pressure and the enthalpy. However, for nonequilibrium flow conditions, such a procedure is not possible. Under some conditions, the number densities of the excited states may instead be determined using the Boltzmann distribution for the electronically, vibrationally, and rotationally excited states. In addition, as described in Ref. 5, the number density of the electronically excited states can be calculated by solving the Master equations. The main assumption in this approach is that a quasi-steady state (QSS) exists for the number density of the excited species. The assumption requires the electronic excitation rate coefficients to be much faster than the timescales for diffusion and for changes in overall properties. Under such conditions, the nonequilibrium flow properties, which are the species number densities, the rotational, the vibrational, and the electronic temperatures, must be known. Then the vibrationally and rotationally excited state number densities are computed using the Boltzmann distribution within these levels.

However, the present study departs from this approach by computing directly the nonequilibrium number density of the electronically and vibrationally excited state species. This approach allows the direct assessment of the validity of the QSS theory, especially in high-altitude regimes where the chemical processes become rare. The present method can also be very useful in helping to understand the nonequilibrium processes that the excited species undergo by providing information about their rotational and vibrational relaxation phenomena. In fact, in NEQAIR, the vibrational, rotational, and electronic temperatures of the bulk flow or of the ground state species are used to compute the number density of the electronically, rotationally, and vibrationally excited states. In reality, in the conditions of highly nonequilibrium flows, the internal temperatures of the ground state species or those of the bulk flow may be very different from the temperatures of the excited states. In such conditions, the approximation used so far in NEQAIR can lead to errors by orders of magnitude. In the case of the OH molecule, it was found that the ground state species undergoes vibrational energy transfer collisions with rates slower than for the A state, OH(A), by about a factor of 100 (Ref. 6). Therefore, the main goal of the present study is to develop a reliable method for signature predictions at high-altitude conditions.

The outline of the present study is as follows: First, the physical models and numerical algorithms developed for the DSMC analysis are discussed. Then the nonequilibrium radiation code used in this study is briefly described. The model of vibrational energy transfer of the electronically excited state is introduced. In terms of results, general properties of the DSMC flowfield solutions are presented. Results obtained with the new nonequilibrium radiation model are compared with the NEQAIR model. Direct comparison of the predicted peak emissions and spectra with the BSUV-2 data are presented. Finally, the flowfield properties that include the rotational and vibrational temperatures of OH(A) are presented, and the emission predictions are analyzed in terms of the OH(A) rotational temperature dependence.

Numerical Models

The numerical models employed in the present work are described in this section. The physical models implemented in the DSMC code are first considered. The new nonequilibrium radiation model is then introduced, and finally the vibrational energy transfer of OH(A) is presented.

Physical Models

The DSMC code employed in the present study is based on the vectorized algorithm described in Ref. 7. The code includes finite rates of rotational and vibrational relaxation and dissociation, exchange, and recombination chemical reactions. A key development in the code is the implementation of a numerical weighting scheme that allows accurate and efficient simulation of trace species.[8] For the altitude range of interest here, the weighting scheme is needed to resolve the excited states, OH(A, $v' = 0, 1, 2$), and their precursors, OH and H_2O. It will be found from computations that the electronically and vibrationally excited state species, OH(A, $v' = 0, 1, 2$), exist in the flows at mole fractions of less than 10^{-9}, and these conditions are handled efficiently by the new weighting scheme. However, for any OH(A, $v' = 0, 1, 2$) particles to exist in the flows, they must be produced through collisional excitation. For the altitudes of interest here (80–100 km), there are few intermolecular collisions, and therefore the occurrence of possible collision events is very rare. As described in Ref. 2, whenever a collision involving an OH particle has sufficient energy to allow electronic and vibrational excitation, the reaction probability is set to unity. The numerical weights of the products are then adjusted to ensure conservation of mass. A special procedure is employed for these excitation collisions whereby several OH(A) particles are created instead of just one. Once again, the numerical weight of each particle is adjusted to conserve total mass. Using this procedure, it is possible to maintain thousands of OH(A, $v' = 0, 1, 2$) particles in the simulation. The spontaneous deexcitation reactions

$$\mathrm{OH}(A, v' = 0, 1, 2) \rightarrow \mathrm{OH} + h\nu \tag{1}$$

and the predissociation reaction

$$\mathrm{OH}(A, v' = 2) \rightarrow \mathrm{O} + \mathrm{H} \tag{2}$$

are implemented in the DSMC code using the algorithm described in Ref. 2.

The observed OH ultraviolet emission is from the $A \rightarrow X$ transition only. Therefore, it is relatively simple to include the production and quenching of the electronically and vibrationally excited states directly in the DSMC flowfield simulations. An 11-species reacting flow model is employed for the species N_2, N, O_2, O, and NO; H_2O, OH, and H; and electronically and vibrationally excited states OH(A, $v' = 0, 1, 2$). The maximum vibrational levels in the computations are fixed to $v' = 2$ because the experimental spectra show no features of vibrational levels greater than 2. In addition to the air reactions,[7] the hydrogenated species undergo the reactions listed in Table 1. Note that the quenching and deexcitation coefficient rates are from Ref. 4, and the reverse reactions coefficient rates are then computed using the principle of balance at equilibrium. The reactions are simulated by the DSMC code using the total collision energy form of the generalized collision energy model.[9] In previous studies, it was shown that prediction of ultraviolet emissions was sensitive to the model assumed for interaction of the gas with the vehicle surface.[2,10] It was found in Ref. 10 that the best agreement of prediction with experimental data occurred for the translational accommodation coefficient of 0.85. This value is consistent with molecular beam experiments. The rotational and vibrational accommodation coefficients were then set, respectively, to 0.5 and 0.1. The rotational accommodation coefficient is also consistent with the observed molecular beam, and the vibrational accommodation coefficient was estimated. In the present work, these values are retained and the surface temperature is taken as 500 K as measured during the BSUV-2 flight. It is also shown in Ref. 2 that the prediction of ultraviolet emission for OH was sensitive to the freestream concentration. Therefore, the concentrations of the hydrogenated species obtained from a model atmosphere[11] and used in Ref. 2 are retained here and listed in Table 2.

Nonequilibrium Radiation Model

The nonequilibrium radiation code described in Ref. 3 and employed for prediction of emission from flowfield solutions was discussed and verified in Ref. 4 for OH, comparing the measured spectra with the predicted emissions. The common assumption made in the NEQAIR code is that the QSS exists for the number densities of the electronically excited species and a single rotational and vibrational temperature model is employed. The validity of the QSS assumption for high-altitude flows was assessed in Ref. 2 using the number density of electronic state species from the DSMC computation. In that approach, the number density of the rotationally and vibrationally excited state was computed using the Boltzmann

Table 1 OH kinetics mechanism

Reaction	Rate coefficient, m^3 molecule^{-1} s^{-1}; $K = AT^N e^{(-E/kT)}$		
	A	N	E/k, K
$H_2O + N_2 \rightarrow OH + H + N_2$	5.81×10^{-15}	0.00	−53,000.0
$H_2O + O_2 \rightarrow OH + H + O_2$	1.13×10^{-07}	−1.31	−59,400.0
$H_2O + O \rightarrow OH + H + O$	1.13×10^{-07}	−1.31	−59,400.0
$OH + N_2 \rightarrow O + H + N_2$	1.25×10^{-15}	0.06	−51,000.0
$OH + O_2 \rightarrow O + H + O_2$	1.25×10^{-15}	0.06	−51,000.0
$OH + O \rightarrow O + H + O$	1.25×10^{-15}	0.06	−51,000.0
$H + O_2 \longleftrightarrow OH + O$	3.65×10^{-16}	0.00	−8,450.0
$O + H_2O \longleftrightarrow OH + OH$	1.13×10^{-16}	0.00	−9,240.0
$OH + N_2 \rightarrow OH(A, v' = 0) + N_2$	9.40×10^{-17}	−0.37	−46,600.0
$OH + O_2 \rightarrow OH(A, v' = 0) + O_2$	2.70×10^{-15}	−0.37	−46,600.0
$OH + N_2 \rightarrow OH(A, v' = 1) + N_2$	2.30×10^{-19}	0.27	−51,173.0
$OH + O_2 \rightarrow OH(A, v' = 1) + O_2$	6.68×10^{-18}	0.27	−51,173.0
$OH(A, v' = 0) + N_2 \rightarrow OH + N_2$	1.64×10^{-19}	0.50	687.0
$OH(A, v' = 0) + O_2 \rightarrow OH + O_2$	4.76×10^{-18}	0.50	450.0
$OH(A, v' = 1) + N_2 \rightarrow OH + N_2$	2.17×10^{-19}	0.50	687.0
$OH(A, v' = 1) + O_2 \rightarrow OH + O_2$	6.31×10^{-18}	0.50	450.0
$OH(A, v' = 0) + N_2 \rightarrow OH(A, v' = 1) + N_2$	5.65×10^{-18}	0.50	−4,573.0
$OH(A, v' = 0) + O_2 \rightarrow OH(A, v' = 1) + O_2$	9.66×10^{-19}	0.50	−4,573.0
$OH(A, v' = 0) + N_2 \rightarrow OH(A, v' = 2) + N_2$	7.46×10^{-18}	0.50	−9,146.0
$OH(A, v' = 0) + O_2 \rightarrow OH(A, v' = 2) + O_2$	2.43×10^{-19}	0.50	−9,146.0
$OH(A, v' = 1) + N_2 \rightarrow OH(A, v' = 2) + N_2$	8.01×10^{-18}	0.50	−4,573.0
$OH(A, v' = 1) + O_2 \rightarrow OH(A, v' = 2) + O_2$	9.20×10^{-19}	0.50	−4,573.0
$OH(A, v' = 1) + N_2 \rightarrow OH(A, v' = 0) + N_2$	5.37×10^{-18}	0.50	0.0
$OH(A, v' = 1) + O_2 \rightarrow OH(A, v' = 0) + O_2$	9.17×10^{-19}	0.50	0.0
$OH(A, v' = 2) + N_2 \rightarrow OH(A, v' = 0) + N_2$	6.71×10^{-18}	0.50	0.0
$OH(A, v' = 2) + O_2 \rightarrow OH(A, v' = 0) + O_2$	2.18×10^{-19}	0.50	0.0
$OH(A, v' = 2) + N_2 \rightarrow OH(A, v' = 1) + N_2$	7.61×10^{-18}	0.50	0.0
$OH(A, v' = 2) + O_2 \rightarrow OH(A, v' = 1) + O_2$	8.74×10^{-19}	0.50	0.0
	Einstein coefficient, s^{-1}		
$OH(A, v' = 0) \rightarrow OH + h\nu$	1.44×10^{6}		
$OH(A, v' = 1) \rightarrow OH + h\nu$	1.36×10^{6}		
$OH(A, v' = 2) \rightarrow OH + h\nu$	1.35×10^{6}		
Predissociation	*Rate, s^{-1}*		
$OH(A, v' = 2) \rightarrow O + H$	3.70×10^{6}		

Table 2 Flow conditions

H, km	ρ_∞, kg m^{-3}	T_∞, K	X_{H_2O}	X_{OH}	X_H
80	2.00×10^{-5}	181	5.6×10^{-6}	4.3×10^{-9}	2.0×10^{-7}
88	5.11×10^{-6}	195	3.0×10^{-6}	1.2×10^{-9}	7.0×10^{-6}
94	1.30×10^{-6}	177	1.2×10^{-6}	3.0×10^{-10}	9.0×10^{-6}
100	5.68×10^{-7}	185	7.2×10^{-7}	2.0×10^{-10}	1.0×10^{-5}

distribution. The number density of the upper state in the spontaneous emission modeling is then written as

$$n_u = n_e \frac{(2J' + 1)}{Q_{vr}} \exp\left\{-\frac{hc}{k}\left[\frac{G'(v')}{T_v} + \frac{F'(J')}{T_r}\right]\right\} \tag{3}$$

The present work, however, departs from this approach by calculating directly from the DSMC code the number densities of the electronically and vibrationally excited states. In this new approach, the number density of the upper state is written as

$$n_u = n_{v'} \frac{(2J' + 1)}{Q_r} \exp\left\{-\frac{hc}{k}\left[\frac{F'(J')}{T_r}\right]\right\} \tag{4}$$

In addition to an assessment of the QSS assumption, the new model allows direct assessment of the usual assumption made in NEQAIR that the rotational and vibrational temperatures of the excited state are the same as those of the bulk flow or of the ground state species.

Rotational and Vibrational Energy Transfer of OH(A)

Collisional transfer of rotational and vibrational energies of OH(A) is the topic of interest in this section. Simulating directly in the DSMC code the production and quenching of OH(A) provides the opportunity to study in detail the rotational and vibrational energy transfer. From the exchange reaction

$$OH(A, v' = 1) + M \rightarrow OH(A, v' = 0) + M \tag{5}$$

where $M \equiv N_2, O_2$, we can define the vibrational relaxation time τ as

$$\frac{1}{\tau} = n_x K_{10}\left[1 - \exp\left(\frac{-\theta_v}{T}\right)\right] \simeq \frac{n_x K_{10} \theta_v}{T} \tag{6}$$

where K_{10} is the vibrational excitation rate related to the $v' = 1 \rightarrow 0$ vibrational transition cross sections, which are reported in Ref. 4 and listed in Table 1. The vibrational relaxation times of OH(A) and OH with N_2 as a colliding partner are shown in Fig. 1. It is noted that the vibrational relaxation time of OH(A) is orders of magnitude lower than that of OH, which indicates the OH vibrational energy transfer rate to be slower than for the A state, OH(A). The rotational relaxation times of OH and OH(A) are assumed to be the same.

The rotational and vibrational energy transfer are then implemented in the DSMC code in addition to the other molecules using the algorithms described in Refs. 12 and 13. However, for vibrational energy transfer modeling, care must be taken when simulating both vibrational energy exchange and chemical exchange reactions between OH(A, $v' = 0, 1, 2$). In fact, the exchange reaction processes involving OH(A, $v' = 0, 1, 2$) also characterize the vibrational energy exchange phenomena. Because the vibrational levels of OH(A) are each treated as if they were separate chemical species and the vibrational relaxation is then treated as a chemical reaction, no additional vibrational relaxation process is applied to OH(A).

Results

The presentation of results is divided into three sections: 1) variation of flowfield properties over the altitude range of interest,

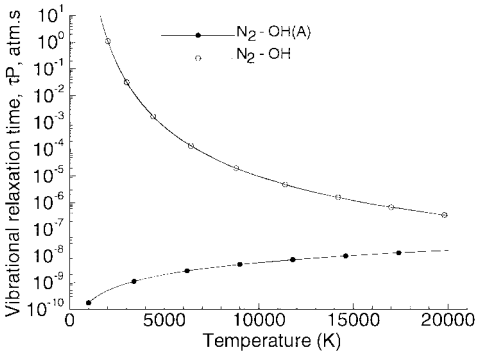

Fig. 1 OH and OH(A) vibrational relaxation times as a function of temperature.

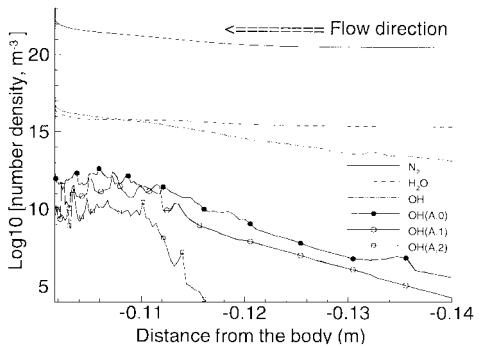

a)

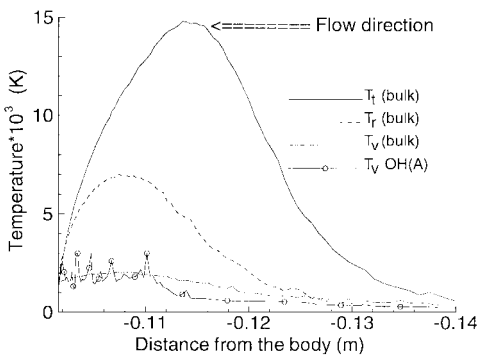

b)

Fig. 2 a) Number densities and b) temperatures along the stagnation streamline at 80-km altitude.

2) comparisons of predicted emissions using the new nonequilibrium radiation model with the NEQAIR model predictions and BSUV-2 flight data, and 3) presentation of general flow properties including OH(A) rotational and vibrational temperatures and sensitivity of predicted emissions to OH(A) rotational temperature.

As in the previous computational studies of the BSUV-2 flight, only flow over the 10-cm-radius spherical nose of the vehicle is simulated. The velocity is in every case 5.1 km/s, and four different altitudes are considered: 80, 88, 94, and 100 km. The hydrogenated species mole fractions, obtained from a model atmosphere presented in Ref. 11, are listed in Table 2. In all cases, the accommodation coefficients for the three energy modes (translation, rotation, and vibration) are set, respectively, to $\alpha_t = 0.85$, $\alpha_r = 0.5$, and $\alpha_v = 0.1$, and the surface temperature is taken as 500 K as measured during the BSUV-2 flight. It is also necessary to note that the values of the accommodation coefficients of the internal energy modes do not influence the radiation prediction.

Flowfield Properties

The computed temperatures and number densities are shown in Figs. 2 and 3 for altitudes of 80 and 100 km. The results show the shock layer becoming thicker at higher altitudes and that a large degree of thermal nonequilibrium exists for the altitudes investigated.

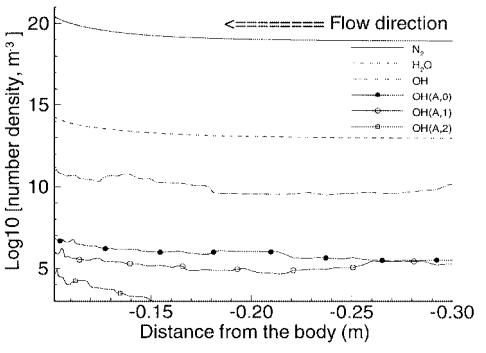

a)

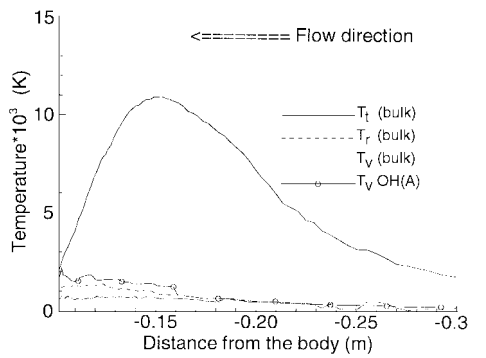

b)

Fig. 3 a) Number densities and b) temperatures along the stagnation streamline at 100-km altitude.

At 80 km, the extent of the chemistry for some of the species is illustrated in Fig. 2a, where OH and OH(A, $v' = 0, 1, 2$) number density profiles are included. However, at 100-km altitude, the number densities of species are almost flat, indicating the relative importance of diffusion over chemical processes, and the peak number density of OH(A, $v' = 0$) is reduced from 10^{12} m^{-3} at 80 km to about 10^{7} m^{-3} at 100 km. The peak values of the temperatures are also considerably reduced, indicating the effect of rarefaction. The effect of rarefaction is also illustrated in Fig. 3a by the OH(A, $v' = 2$) number density profile. In fact, for any OH(A, $v' = 2$) particle to exist in the flow, it must be produced through OH(A, $v' = 0$) or OH(A, $v' = 1$) collisional excitation. Despite the fact that several OH(A, $v' = 2$) particles are assumed to be created at each collisional event, very few OH(A, $v' = 2$) particles are simulated after several thousand time steps. Note that, despite the efficiency of the numerical model in handling the trace species simulation, the statistical noise related to OH(A) properties are significant. For clarity of presentation, the shock layer domain is reduced in Figs. 3a and 3b. This explains the fact that the temperatures do not reach the freestream value.

In Figs. 2b and 3b, the vibrational temperature of OH(A) is computed from the predicted number density n_0 of the ground state, OH(A, $v' = 0$), and the first excited state, OH(A, $v' = 1$), number density n_1 using the Boltzmann distribution:

$$T_v = -\frac{\Delta E_v / k}{\ln(n_1/n_0)}$$

where ΔE_v characterizes the difference between the two energy levels. It is noted that the vibrational temperature computed in this manner is relatively constant.

OH Emission

In Figs. 4a and 4b, the computed spectra at 80 and 100 km are compared with the results obtained using the QSS theory. It is shown that the spectra computed using the QSS theory do not simulate the vibrational transition of OH(A) 1–0 at 0.28 μm and the shoulder of the OH(A) 0–0 vibrational transition at 0.31 μm is too narrow. The absence of the 1–0 feature in the QSS theory is explained by the inaccuracy of the vibrational temperature used in this model. Note that the new radiation model does not use the vibrational temperatures but rather the number densities computed from the flowfield

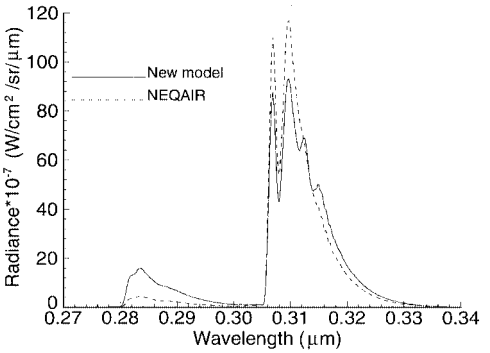

a) At 80-km altitude

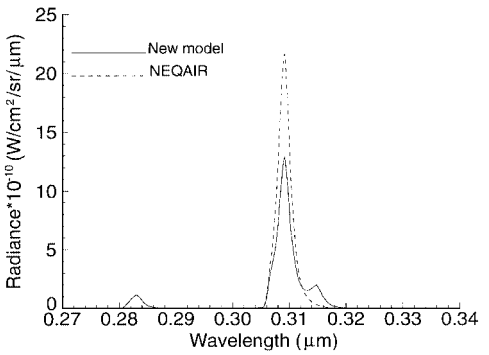

b) At 100-km altitude

Fig. 4 Comparison between DSMC and NEQAIR of the ultraviolet spectra.

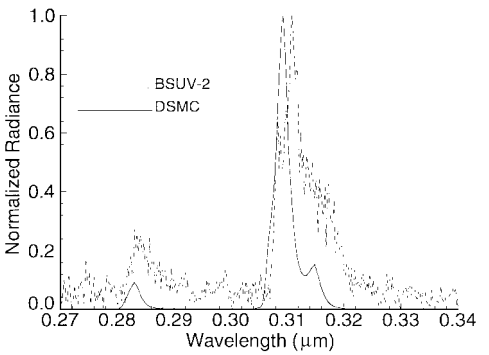

Fig. 5 Normalized ultraviolet spectra at 100-km altitude.

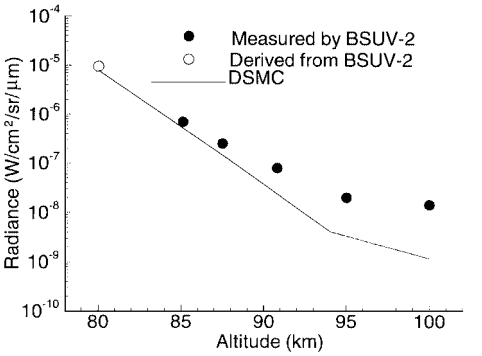

Fig. 6 Peak emission at 0.31 μm as a function of altitude.

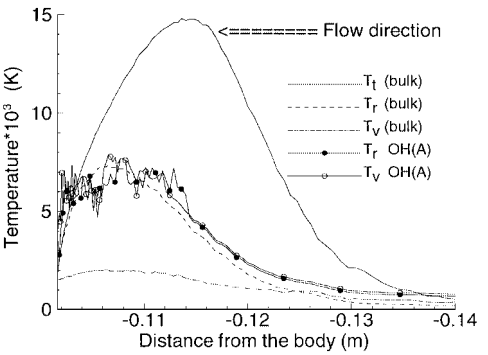

a) At 80-km altitude

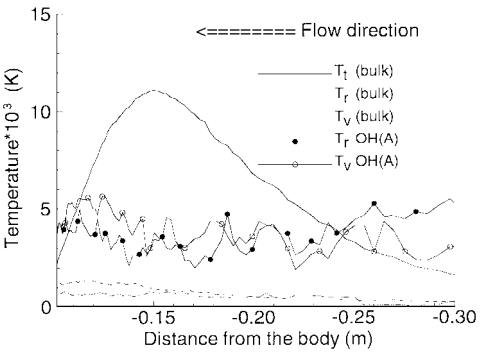

b) At 100-km altitude

Fig. 7 Temperatures along the stagnation streamline.

simulations. The splitting of the 0–0 peak and the left-hand shoulder of the 0.31-μm peak depend on the rotational temperature, and the disappearance of the 0–0 peak at 100 km in both models is due to the small value of the rotational temperature.

In Fig. 5, the spectrum computed with the new model is compared with the BSUV-2 flight data at 100 km. Although the comparison is reasonable, the peak value at 0.28 μm in the prediction is relatively small compared with the data, and the left-hand shoulder of the 0.31-μm peak has almost disappeared. One possible explanation for the relatively small value of the predicted peak at 0.28 μm is inaccuracy in the OH(A) collision cross sections. In fact, the ratio of the peak heights at 0.28 μm ($v' = 1 \rightarrow v'' = 0$) and 0.31 μm ($v' = 0 \rightarrow v'' = 0$) depends on the vibrational temperature. The collision cross sections for vibrational energy exchange reactions, listed in Table 1, were measured for temperatures of about 3000 K, and the use of these data for flow conditions with translational temperatures around 10,000 K may lead to errors. The disappearance of the left-hand shoulder of the 0.31-μm peak is explained by the relatively small value of the computed rotational temperature, indicating that the simulation cannot predict correctly all spectral features of the data. As shown in Fig. 3b, the rotational temperature is about 1500 K, whereas the spectral data indicate the rotational and vibrational temperatures to be on the order of 3000 and 7000 K, respectively.

The peak emissions at 0.31 μm as a function of altitude are compared in Fig. 6. The experimental data are from the spectra measured by BSUV-2. The spectral peak height at 80 km is derived from calculation and measurement data using physical arguments.[4] The agreement is quite good at all altitudes lying within a factor of 2 at 88 km and about 10 at 100 km. Recall that there is about a factor of 2 uncertainty in the BSUV-2 data.

OH(A) Flow Properties and Emission Sensitivity to Rotational Temperature

To assess the validity of the single rotational and vibrational temperature assumption employed in NEQAIR, profiles of bulk flow and OH(A) temperatures along the stagnation streamline are shown in Figs. 7a and 7b for altitudes of 80 and 100 km. Note that the vibrational temperatures obtained through vibrational relaxation of OH(A) and reproduced in Figs. 7a and 7b are different from the temperatures in Figs. 2b and 3b, which were obtained assuming a Boltzmann distribution. It is seen in Fig. 7b that the internal temperatures of OH(A) are very high in the freestream. This is explained by the importance of the diffusion process. In fact, due to rarefaction effects at 100 km, OH(A) particles produced through chemical processes diffuse all along the stagnation streamline from their point of formation, preventing OH(A) internal temperatures from converging to the freestream value. It is also clearly shown that the

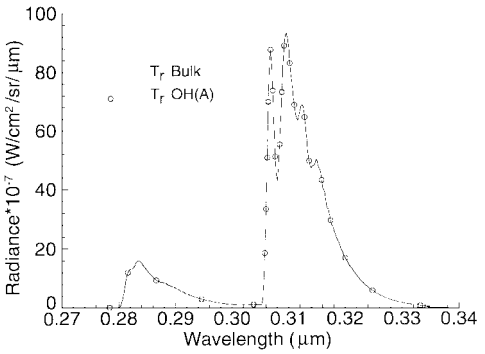

a) At 80-km altitude

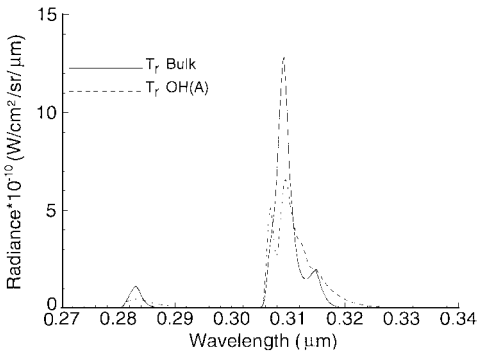

b) At 100-km altitude

Fig. 8 Rotational temperature dependence of the ultraviolet spectra.

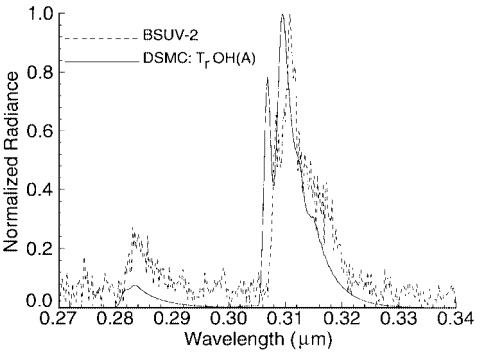

a) OH(A) rotational temperature

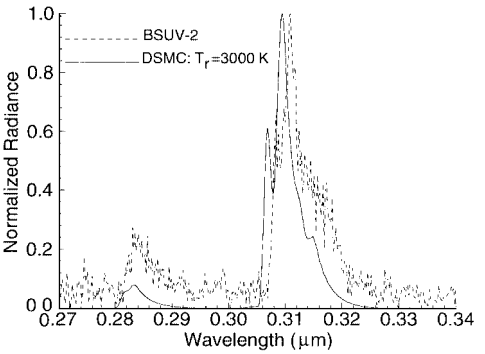

b) Rotational temperature of 3000 K

Fig. 9 Comparison of the normalized ultraviolet spectra at 100 km.

internal temperatures of OH(A) are different from those of the bulk gas. However, at 80 km where there is a sufficient number of collision events, the two rotational temperatures are very similar. The two vibrational temperatures are quite different; the OH(A) vibrational temperature is very close to its rotational temperature, and the peak value is about 7500 K. At 100 km, simulations show that OH(A) internal temperatures are very high compared with the bulk gas. The OH(A) rotational and vibrational temperature peaks are about 4000 and 5000 K, whereas the bulk gas flow simulation indicates the flow rotational and vibrational temperatures to be about 1500 and 800 K, respectively (Fig. 3b). The present results also show that the OH(A) vibrational temperature becomes important compared with the rotational temperature, in agreement with the BSUV-2 flight experiments. However, the present results are different by about 1000 K from the spectral data, which indicate the OH(A) rotational and vibrational temperatures to be on the order of 3000 and 7000 K, respectively. To explain the discrepancy, further results were computed by varying the internal energy mode accommodation coefficients. However, the results obtained for several tests indicate that the internal temperatures do not vary much with accommodation coefficients. It is concluded that the internal temperatures of OH(A) are related to OH(A) chemical processes, and this conclusion will be confirmed in the following discussions. In simulating OH(A) production from OH molecules using the generalized collision energy model, any excess collision energy above the activation energy is equipartitioned into the rotational and vibrational modes. This approach is partially verified through the relatively good agreement obtained with the BSUV-2 spectra.

Sensitivity of the emission predictions to the OH(A) rotational temperature is considered here. The new nonequilibrium radiation model is again considered. In contrast to results shown earlier, the rotational temperature of the bulk gas in the emission prediction is replaced by the OH(A) rotational temperature. As seen from Fig. 8b at 100 km, the splitting of the 0–0 peak and the right-hand shoulder of the 0.31-μm peak vary considerably with the rotational temperature. At 80 km (Fig. 8a), this variation is insignificant, indicating that the OH(A) rotational temperature is the same as the bulk rotational temperature. In Fig. 9a, the spectrum computed using the OH(A) rotational temperature is compared with the BSUV-2 data at 100 km. An improvement is obtained with the left-hand shoulder of the 0.31-μm peak, which has increased significantly in the calculated spectrum. However, this peak value is relatively high compared with the experimental data, indicating that the OH(A) rotational temperature is too high in the numerical simulation. To assess this conclusion, the emission is predicted at 100-km altitude assuming a rotational temperature of 3000 K. Figure 9b indicates a decrease in the right-hand shoulder of the 0.31-μm peak, which is now in good agreement with the BSUV-2 flight data. This result confirms the OH(A) rotational temperature to be on the order of 3000 K. Using the OH(A) rotational temperature, it is noted that the peak emission at 0.31 μm is reduced, especially at 100 km where the OH(A) and the bulk gas rotational temperatures have a large discrepancy.

Assuming the rotational temperature of OH(A) to be 3000 K at 100-km altitude and comparing the predicted peak with the flight data, an estimate of the OH freestream mole fraction is then obtained. The derived OH mole fraction is about 4.0×10^{-9}. This value is about 20 times higher than the value reported in Table 2. Using the same procedure, the freestream water mole fraction is derived at 80 km through comparison of the predicted peak with the derived 80-km data point. The derived water mole fraction is about 6.1×10^{-6} and very close to the data reported in Table 2. It was found in Ref. 2 that, at low altitudes, such as 80 and 88 km, the emission predictions were directly proportional to the ambient water mole fraction. However, at high altitudes, such as 94 and 100 km, where the effects of rarefaction are very significant, the emission predictions were directly proportional to the OH freestream mole fraction. Considering these results, the ambient water mole fraction and the OH freestream mole fraction are also derived at 88 and 94 km. The water mole fraction is found to be on order of 4.2×10^{-6} at 88 km, and the OH mole fraction is about 6.0×10^{-9} at 94 km. The derived mole fractions of the hydrogenated species are reported in Table 3.

Using the mole fractions of the hydrogenated species listed in Table 3, the DSMC method is applied to compute the flowfield properties, and the new nonequilibrium radiation model is used to predict OH emission over the altitude range of 80–100 km. In Fig. 10, the peak emissions at 0.31 μm as a function of altitude are compared with data taken from the spectra measured on the BSUV-2 flight. Clearly, excellent agreement is obtained, suggesting that the hydrogenated species mole fractions experienced in the BSUV-2 flight experiments are within the data listed in Table 3.

Table 3 Derived freestream mole fractions

H, km	X_{H_2O}	X_{OH}
80	6.1×10^{-6}	——
88	4.2×10^{-6}	——
94	——	6.0×10^{-9}
100	——	4.0×10^{-9}

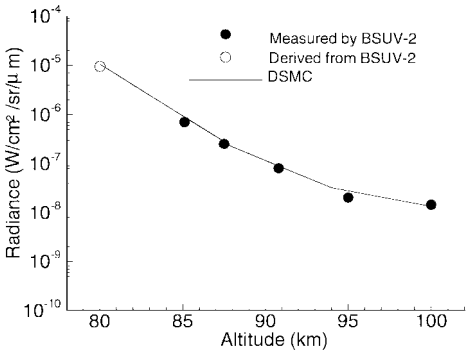

Fig. 10 Peak emission at 0.31 μm as a function of altitude using the derived OH mole fractions.

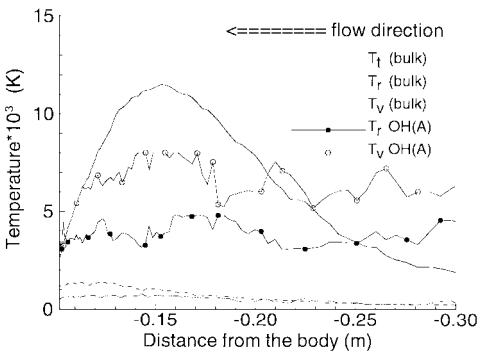

Fig. 11 Temperatures along the stagnation streamline at 100-km altitude using the derived OH mole fractions.

However, as mentioned previously, the quenching coefficient rates can also explain the discrepancy observed between the predicted spectra and the experimental data. The derived mole fractions must then be considered representative rather than definitive.

Considering once again the flow and OH(A) properties at 100-km altitude, it is shown in Fig. 11 that the OH(A) rotational and vibrational temperatures are in good agreement with the temperatures indicated by the BSUV-2 spectral data. It is noted that the internal temperatures of OH(A) obtained with the new freestream mole fraction are higher than those reported in Fig. 7b. In fact, because the OH mole fraction is increased, the occurrence of collisional excitation is also increased and so are the number of particles in high rotational and vibrational levels. This result also demonstrates that, in high-altitude conditions, OH(A) internal energy temperatures are related to the chemical processes rather than collisional energy transfer.

Summary

The direct simulation Monte Carlo method was used to predict the number densities of electronically and vibrationally excited state species of OH in nonequilibrium, hypersonic flight conditions. The conditions corresponded to the BSUV-2 flight experiment over the altitude range of 80–100 km.

The profiles of OH(A, $v' = 0, 1, 2$) were then used to predict the ultraviolet spectra from OH(A). The comparisons of both the peak value and the overall spectral shape were found to be in good agreement with the flight data. However, the ratio of the peaks at 0.28 μm showed some disagreements that could be related to the inaccuracy of the quenching and exchange collision cross sections at high temperature. In addition, the left-hand-shoulder height at 0.31 μm showed disagreements at high altitude that are due partly to inaccuracy in computing rotational temperatures. Nevertheless, the present study represents a significant improvement compared with NEQAIR.

Comparisons of OH(A) rotational and vibrational temperatures with the bulk gas flow values showed that at the lower-altitude conditions the two rotational temperatures were in good agreement, whereas the vibrational temperatures were very different. Furthermore, it was also shown that at high altitudes the OH(A) internal temperatures were higher than those of the bulk gas. Using OH(A) rotational temperatures, the emission was computed that reproduced both the spectral shapes and the peak emission dependence on the rotational temperature. Comparisons of the emission predictions with the BSUV-2 flight experiments allowed the estimation of H_2O and OH ambient mole fractions over the range of altitudes of interest. The H_2O ambient mole fractions were found to be close to values from a model atmosphere, whereas OH freestream mole fractions were found to be higher by about a factor of 20. Using the derived freestream mole fractions, the flowfield was then computed, and the emissions predicted. Good agreement was obtained with the flight data for both the peak emission and the overall spectra. With the new freestream mole fractions, agreement was obtained between OH(A) internal temperatures and those indicated by the spectral data.

Acknowledgment

This work is funded by the U.S. Air Force Office of Scientific Research under Grant F49620-96-1-0091.

References

[1]Erdman, P. W., Zipf, E. C., Espy, P., Howlett, L. C., Levin, D. A., Collins, R. J., and Candler, G. V., "Measurements of Ultraviolet Radiation from a 5-km/s Bow Shock," *Journal of Thermophysics and Heat Transfer*, Vol. 8, No. 3, 1994, pp. 441–446.

[2]Kossi, K. K., Boyd, I. D., and Levin, D. A., "Direct Simulation of Ultra-Violet Emission from the Hydroxyl Radical," *Journal of Thermophysics and Heat Transfer*, Vol. 12, No. 1, 1998, pp. 223–229.

[3]Park, C., "Calculation of Nonequilibrium Radiation in the Flight Regimes of Aero-Assisted Orbital Transfer Vehicles," *Thermal Design of Aero-Assisted Orbital Transfer Vehicles*, edited by H. F., Nelson, Vol. 96, Progress in Astronautics and Aeronautics, AIAA, New York, 1985, pp. 395–418.

[4]Levin, D. A., Laux, C., and Kruger, C., "A General Model for the Spectral Calculation of OH Radiation in the Ultraviolet," *Journal of Quantitative Spectroscopy and Radiative Transport* (to be published).

[5]Park, C., *Nonequilibrium Hypersonic Aerothermodynamics*, Wiley, New York, 1990, pp. 89–118.

[6]Copeland, R. A., Wise, M. L., and Crosley, D. R., "Vibrational Energy Transfer and Quenching of OH($A^2\Sigma^+$, $v' = 1$)," *Journal of Physical Chemistry*, Vol. 92, No. 20, 1988, pp. 5710–5715.

[7]Boyd, I. D., and Gokcen, T., "Computation of Axisymmetric and Ionized Hypersonic Flows Using Particle and Continuum Methods," *AIAA Journal*, Vol. 32, No. 9, 1994, pp. 1828–1837.

[8]Boyd, I. D., "Conservative Species Weighting Scheme for the Direct Simulation Monte Carlo Method," *Journal of Thermophysics and Heat Transfer*, Vol. 10, No. 4, 1996, pp. 579–585.

[9]Boyd, I. D., Bose, D., and Candler, G. V., "Monte Carlo Modeling of Nitric Oxide Formation Based on Quasi-Classical Trajectory Calculations," *Physics of Fluids*, Vol. 9, April 1997, pp. 1162–1170.

[10]Boyd, I. D., Phillips, W. D., and Levin, D. A., "Sensitivity Studies for Prediction of Ultra-Violet Radiation in Nonequilibrium Hypersonic Bow-Shock Waves," *Journal of Thermophysics and Heat Transfer*, Vol. 12, No. 1, 1998, pp. 38–44.

[11]Brasseur, G., and Solomon, S., *Aeronomy of the Middle Atmosphere*, 2nd ed., Reidel, Dordrecht, The Netherlands, 1986, pp. 442, 443.

[12]Bergemann, F., and Boyd, I. D., "New Discrete Vibrational Energy Model for the Direct Simulation Monte Carlo Method," *Rarefied Gas Dynamics*, Vol. 158, Progress in Astronautics and Aeronautics, AIAA, Washington, DC, 1994, pp. 174–183.

[13]Boyd, I. D., "Analysis of Rotational Nonequilibrium in Standing Shock Waves of Nitrogen," *AIAA Journal*, Vol. 28, No. 11, 1990, pp. 1997, 1998.

R. G. Wilmoth
Associate Editor